International Conference on Computational Methods in Marine Engineering
MARINE 2011
L.Eça, E. Oñate, J. García, T. Kvamsdal and P. Bergan (Eds)

RANS PREDICTIONS OF ROLL VISCOUS DAMPING OF SHIP HULL SECTIONS

F.Jaouen*, A.H.Koop#, G.Vaz# and P.Crepier&

* #Maritime Research Institute Netherlands (MARIN)
P.O. Box 28
6700 AA Wageningen, The Netherlands
e-mail: f.jaouen@marin.nl, www.marin.nl

&ENSTA-Bretagne
2, rue Francois Verny
Brest 29806 Cedex 09, France

Key words: URANS, roll-damping, bilge-keels, seakeeping, ReFRESCO, verification, validation

Abstract. The unsteady flow around a forced rolling hull section with and without bilge keels is computed using URANS code ReFRESCO. In this paper, extensive studies have been carried out in the dependence on grid resolution and time-step size on the linear roll viscous-damping coefficient. The influence of the grid resolution on the viscous-damping coefficient is significant, and relatively fine grids should be used to obtain a grid-converged solution. The coefficient estimates decrease with grid refinement. The influence of the time step is smaller. The numerical results obtained for the rectangular hull with sharp bilges have been compared to classical experimental data by Ikeda. A very good agreement has been found, with deviations lower than 10% for several amplitudes and two periods. For this case, it is confirmed that the viscous-damping coefficient is linear with the roll amplitude. The numerical results obtained for the rectangular hull with triangular-shaped bilge keels have also been compared to available experimental data. A reasonable agreement between ReFRESCO results and the experimental data is found for dimensionless frequencies lower than 0.7. For these values a deviation from the experimental values lower than 10% is observed. For higher dimensionless frequencies, the calculated viscous-damping coefficient highly overestimates the model-tests results, which is expected to be related to non-linear free-surface effects. The viscous damping calculated is linear with the frequency, which is not true for the experiments for frequencies higher than 0.7. For the hull section with bilge keels, a preliminary study on possible scale effects has been performed. One calculation has been carried out for a full-scale Reynolds number corresponding to a geometrical scale factor of 50. The preliminary results showed that the pressure and vorticity fields are very similar for model and full scale. The difference in viscous damping coefficient between model and full scale is of 1.85%.

1 INTRODUCTION

In order to guarantee both safety and comfort of the passengers of a ship, the roll motion of a vessel has to satisfy with safety regulations. Therefore, predicting the roll damping of the vessel is an important consideration for naval architects, because it determines the extreme roll motions of the vessel in a given sea state. As pointed out by Ikeda et al. [1], or Himeno [2], the total roll damping coefficient for a ship hull can be divided into a number of components (if linearization is considered valid): skin-friction stress on the hull, eddy damping due to pressure variations on the hull, wave damping due to free-surface waves and bilge-keel damping. The change in pressure on the hull due to the bilges and bilge keels is highly dominated by viscous effects, especially due to generated eddies formed at the sharp edges of the bilges or bilge keels.

Computational methods based on potential-flow theory are the work-horse tool for predicting motions of a ship in waves, but they cannot predict viscous effects. Nowadays, model tests are believed to give

the most accurate answer. However, model testing is usually expensive and time consuming, making it difficult to investigate the influence of different bilge keel designs. Also, they suffer from possible scale or Reynolds effects. In the industry, a method commonly used is to estimate the viscous damping by applying the empirical formulas established by Ikeda, or to use model tests data based on similar vessels. These methods give fast but rough estimates for the roll damping. The aim of this paper is to show that Computational Fluid Dynamics (CFD) can play an important role in the assessment of damping coefficients, viscous effects and in the understanding of complex flow behavior around the bilges and bilge keels of the hull. CFD may offer a cost-effective method complementary to model tests to obtain damping coefficients with reasonable accuracy and to provide detailed flow visualizations. Therefore, a better understanding of the possibilities and limitations of CFD for determining roll damping and the sensitivity of CFD results for various parameters by hands-on experience is required.

In [3, 4], Yeung studied the hydrodynamic moment applied on a rectangular cylinder fitted with bilge keels. The numerical results of a so-called Free-Surface Random Vortex Method are compared to experimental data. The capability of this method was shown to be reasonably good. In 2008, Yu performed URANS numerical simulations using a in-house CFD code, and the results were compared to the numerical results obtained with the commercial code FLUENT, and to the experimental data of Yeung [3, 4]. The linear roll-damping coefficient was calculated for various frequencies. The dependency of the damping to the frequency was correctly captured, but significant differences were observed. Coarse grids and time-steps and the lack of turbulence modelling may explain the large overpredictions. In [5] it has been shown that URANS code ReFRESCO can accurately predict the roll damping of a hull section with sharp bilges. It was shown that sensitivity studies to discretization errors and iterative convergence errors should be done with care to obtain accurate results. Here, the 2D calculations on the hull section with sharp bilges reported in [5] are re-performed for a larger range of amplitudes and periods. Additionally, calculations are performed on a 2D hull section equipped with triangular shaped bilge keels. For this second case, extensive numerical studies are performed for one roll amplitude with one roll period. A broad range of roll periods are then computed and the numerical results are compared to the experimental results by Yeung [3, 4]. For the hull section with bilge keels, the influence of turbulence modelling and the possible existence of Reynolds effects is briefly investigated.

With the calculations here presented we only study the viscous roll-damping coefficients. The added-mass coefficients have already been studied in [5], they are easy to capture, and potential-flow codes can estimate them as well with reasonable accuracy. Also, in order to study the viscous roll-damping component exclusively due to the flow around the hull, we don't consider the roll-damping component due to free-surface or wave making in the CFD calculations. If this component is not negligible we determine it using a potential-flow code and we can sum it to the other component. This is the same as considering a linearization with respect with the wave-making component. This linearization has been seen to be valid in certain conditions [1]. In a next phase we will consider the wave-making component in the CFD calculations. Modern verification and validation procedures usually applied at MARIN [6, 7] are not applied here, and will also be considered in a next phase of the current work.

The paper is organized as follows: after this introduction, the definitions and theoretical approach to the roll-damping analysis are explained. Afterwards, both the experimental data and the computational setup (geometries, tools, settings, boundary-conditions) are presented. The numerical results on the hull section with sharp bilges are then presented, followed by the case with bilge keels. The paper ends with conclusions and remarks on further work.

2 THEORETICAL FORMULATION

2.1 Definitions

A right-handed cartesian coordinate system is used in this paper. The roll motion of the hull section is forced around the z axis, perpendicular to the hull section. The description of the symbols used in this paper is given in Table 1. To make the comparison between different scales easier, the cyclic frequency of the forced roll motion is made dimensionless as follows:

$$\omega^* = \omega \sqrt{\frac{B}{2g}}. \tag{1}$$

Note that ω^* can be considered as an equivalent Froude number. The flow analysis presented in this paper emphasizes on the pressure and vorticity fields. These are respectively noted C_p and ω_z^*, and are made dimensionless as follows

$$C_p = \frac{p}{0.5 \cdot \rho \cdot V_{ref}^2} = \frac{p}{0.5 \cdot \rho \cdot (R_{BK} \cdot \omega)^2}, \tag{2}$$

$$\omega_z^* = \omega_z \cdot \left(\frac{T}{2\pi} \right). \tag{3}$$

with the reference length R_{BK} the distance between the rotation point and the hull section bilge $R_{BK} = \sqrt{(B/2)^2 + D^2}$.

B	Breadth of the hull [m]	$a_{\phi\phi}$	Added-mass coefficient [-]
D	Draft of the hull [m]	$b_{\phi\phi}$	Damping coefficient [-]
g	Gravitational acceleration [m/s2]	$a^*_{\phi\phi}$	Dimensionless added mass coefficient [-]
T	Forced roll period [m]	$b^*_{\phi\phi}$	Dimensionless damping coefficient [-]
ν	Kinematic viscosity of water [m2/s]	$Re = \frac{V_{ref} B}{\nu}$	Reynolds number [-]
ρ	Density of water [kg/m3]	Re_{ms}	Model-scale Reynolds number [-]
ϕ_0	Forced roll amplitude [rad]	Re_{fs}	Full-scale Reynolds number [-]
ω	Roll cyclic frequency [rad/s]	C_p	Pressure coefficient [-]
ω^*	Dimensionless frequency [-]	ω_z^*	Dimensionless z-vorticity [-]
R_{BK}	Reference length [m]	$V_{ref} = \omega R_{BK}$	Reference velocity [-]

Table 1: Nomenclature

2.2 Roll damping analysis

As referred in the introduction, only the damping due to viscous effects is determined. The wave damping is assumed to be very small for the ratio B/D herein investigated and for dimensionless frequencies lower than 0.6 [8] . The free-surface, and associated wave damping is not considered in the CFD calculations in this paper. Nevertheless, the linearized wave-damping contribution can be estimated accurately using potential-flow codes such as DIFFRAC [9], and added to the viscous-damping coefficient to obtain a total-damping coefficient. The model geometry is mirrored in the water plane and completely submerged in the water. The setup used for the computations is shown on Figure 1.

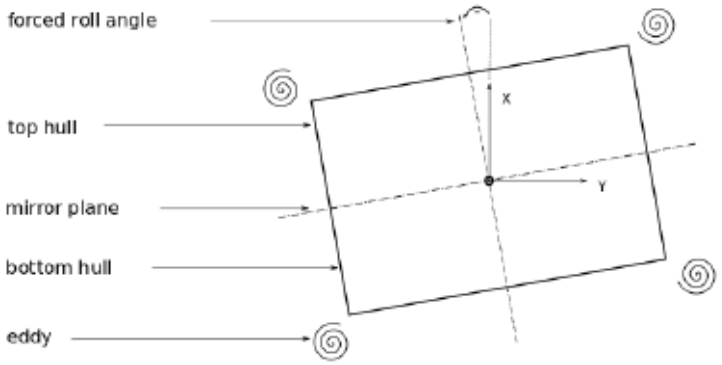

Figure 1: Description of the setup and sign conventions.

A harmonic roll motion is prescribed by moving the hull by a roll angle $\phi(t)$ defined as follows,

$$\phi(t) = \phi_0 \sin \omega t, \tag{4}$$

with ϕ_0 the amplitude of the roll motion and ω the angular frequency. The sign convention can be seen on Figure 1. A start-up function $G(t)$ is applied for the first T_F roll periods of the simulation. This is

necessary to avoid strong transient flows at the earlier time steps of the calculation. The start-up function $G(t)$ is defined by

$$G(t) = \begin{cases} \frac{1}{2}\sin\left(\frac{\omega t}{2T_F} - \frac{1}{2}\pi\right) + \frac{1}{2} & \text{, for} \quad t < T_F T, \\ 1 & \text{, for} \quad t \geq T_F T. \end{cases} \tag{5}$$

The roll angle $\phi(t)$ is then defined by

$$\phi(t) = G(t)\phi_0 \sin \omega t. \tag{6}$$

The prescribed roll angle $\phi(t)$ leads to a hydrodynamic reaction roll moment $M_E(t)$. The equation of motion for uncoupled forced roll motion can be described by the second-order differential equation [8]:

$$a_{\phi\phi}\phi'' + B(\phi, \phi') + C(\phi) = M_E(t), \tag{7}$$

where $a_{\phi\phi}$ is the added mass for roll motion, $B(\phi, \phi')$ the damping moment, $C(\phi)$ the restoring moment, which is equal to zero in the absence of a free surface and gravity, and $M_E(t)$ the excitation/reaction moment. Various forms for the damping moment exist. Here, we consider a so-called equivalent linear form, i.e. $B(\phi, \phi') = b_{\phi\phi}\phi'$, with $b_{\phi\phi}$ the roll damping coefficient. Finally, the equation of motion becomes:

$$a_{\phi\phi}\phi'' + b_{\phi\phi}\phi' = M_E(t). \tag{8}$$

Although the prescribed roll motion $\phi(t)$ is a pure sine (after the start-up phase), the exciting roll moment $M_E(t)$ is not due to effects from viscosity and eddy making. We assume that the reaction roll moment $M_E(t)$ can be approximated by a pure sine function $M_\phi(t)$, which can be expressed as

$$M_\phi(t) = M_0 \sin(\omega t + \epsilon), \tag{9}$$

where M_0 is the amplitude of the roll moment and ϵ indicates the phase angle between the prescribed roll angle and the roll moment. Martin [10] investigated four different sinusoid fitting methods, also described in [8]: the so-called *Morrison method*, the *harmonic-analysis method*, the *least-square method*, and the *weighted least-square method*. In an initial stage of the current work, these four methods have been applied both to the numerical and experimental results. It was concluded that the harmonic-analysis and the least-square methods led to similar results, while the two other methods revealed to be less robust and can give significantly different results. For the study here presented, the harmonic-analysis method is chosen to fit a sinusoid M_ϕ on the computed moment time-trace M_E. The harmonic analysis is based on the calculation of Fourier coefficients, and therefore it should be noted that an extra post-processing step is involved between the computed moment, and the hydrodynamic coefficients. Thus, the linear equation of motion for uncoupled roll motion is given as

$$a_{\phi\phi}\phi'' + b_{\phi\phi}\phi' = M_\phi(t). \tag{10}$$

Developing the previous equation, it is found that the added mass and damping coefficients can be expressed as follows:

$$a_{\phi\phi} = \frac{-M_0\cos(\epsilon)}{\phi_0\omega^2}, \quad b_{\phi\phi} = \frac{M_0\sin(\epsilon)}{\phi_0\omega}. \tag{11}$$

For comparison the hydrodynamic coefficients are normalized by

$$a^*_{\phi\phi} = \frac{a_{\phi\phi}}{\rho\nabla B^2}, \quad b^*_{\phi\phi} = \frac{b_{\phi\phi}}{\rho\nabla B^2}\sqrt{\frac{B}{2g}}, \tag{12}$$

where ∇ is the hull displacement defined as $\nabla = DB$, with D the draft and B the breadth as presented in Figure 2. The hydrodynamic moment M_E on the object is defined by

$$M_E = \int_S (p\mathbf{r} \times \mathbf{n} + \tau\mathbf{r} \times \mathbf{t})\, dS, \tag{13}$$

where $\mathbf{r}$ is the lever-arm vector, i.e. the vector from the axis of rotation to the point of force application. S is the surface of the object, p the pressure and τ the viscous stress on that surface. $\mathbf{n}$ is the unit normal vector pointing into the object, i.e. out of the computational domain and $\mathbf{t}$ is the tangential unit vector. Since a double-body geometry is considered the integral in Equation (13) is only taken over the bottom half of the configuration shown in Figure 4(b).

3 TEST-CASES

3.1 Hull with sharp bilges

The experimental data of Ikeda [11] on the hull section with sharp bilges is used. The model-tests results consist of forced-oscillation tests of a ship hull that spans the whole basin breadth. The ship-hull geometry is shown on Figure 2(a) and its dimensions are $L \times B \times D = 0.80 \times 0.28 \times 0.112m$. The tests were carried out with free surface, which means that the results include a wave-damping component. The rotation axis is located at the free-surface and the hydrodynamic moment applied on the hull has been measured. Two roll periods T=1.0s ($\omega^* = 0.500$) and T=1.5s ($\omega^* = 0.750$) and various roll amplitudes between $\phi_0 = 0.085rad$ (4.87deg) and $\phi_0 = 0.232rad$ (13.3deg) have been measured. The Re number based on the largest frequency of $\omega^* = 0.750$ is $Re = 2.4 \times 10^5$. A comparison between experimental and numerical results is done for both periods/frequencies.

3.2 Hull with bilge keels

The experimental data of Yeung [3, 4] on a hull section with rounded bilges and triangular shaped bilge keels is also considered. The hull and bilge keel geometries are shown on Figure 2(b). Added mass and damping coefficients for a rectangular hull of dimensions $L \times B \times D = 2.44 \times 0.3048 \times 0.1524m$ have been obtained. The tests were carried out with free surface. Three bilge configurations were tested: one hull without bilge keels, one hull with bilge keels length 4% of the hull breadth and one hull with bilge keels length 6% of the hull breadth. For each hull, forced-oscillations model tests have been performed, for two amplitudes $\phi_0 = 0.05rad$ (2.9deg) and $\phi_0 = 0.1rad$ (5.7deg) on a range of periods between T=0.34s ($\omega^* = 2.30$) and T=2.26s ($\omega^* = 0.35$). For this study, the hull section with a bilge-keel length of 4% with a roll amplitude of $0.1rad$ is used. The numerical studies have been performed for one amplitude $\phi_0 = 0.1rad$ and one period $T = 1.55s$ ($\omega^* = 0.505$). The Re number based on the frequency of $\omega^* = 0.505$ is $Re = 2.7 \times 10^5$. Comparison between experimental and numerical results is done for the same amplitude and the complete range of periods/frequencies.

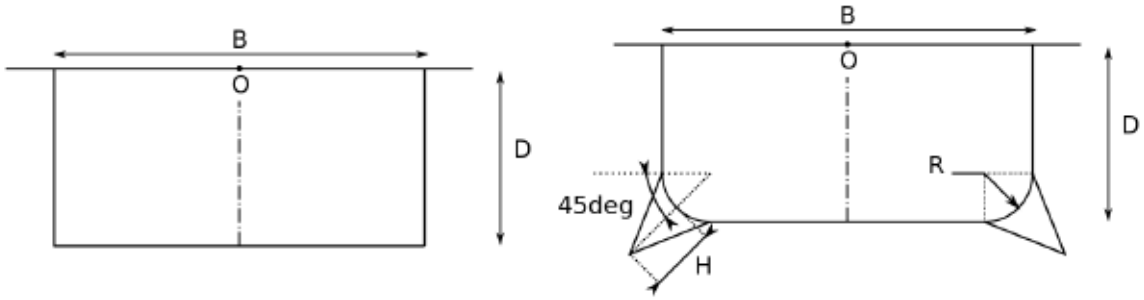

(a) Hull with sharp bilges [11]

(b) Hull with bilge keels [3, 4]

Figure 2: Overview of the geometries used.

4 COMPUTATIONAL SETUP

4.1 Domain and computational grids

Numerical computations are performed for the cases presented in Section 3. For both cases, a circular-shaped cylindrical domain is used for the computations. This computational domain is closed by a circular boundary located at a radius 3m from the centre of rotation. This ensures that the velocity and pressure field generated by the oscillating body is unaffected by the outer-boundary, such as shown in [12]. The grids are three-dimensional with one element in the z-direction, simulating a two-dimensional situation.

For the hull with sharp bilges, five consecutively refined block-structured grids have been constructed using the commercial grid generator package ICEM-CFD [13]. The coarse, coarse-medium, medium, medium-fine and fine grids contain respectively 42K, 97K, 173K and 392K and 698K cells. An overview of the coarse grid is shown in Figure 3. For the hull with bilge keels, four consecutively refined structured grids have been constructed using the grid generator package GridPro [14]. The coarse, medium, fine and

very fine grids contain respectively 10K, 40K, 160K and 800K cells. An overview of the coarse grid is shown in Figure 4. The grids are clustered towards the corners of the 2D hull section, so that the vortices generated at the bilges or bilge keels are accurately captured in space. The quality of GridPro grids is higher due to its smoother stretching and higher orthogonality close to the hull.

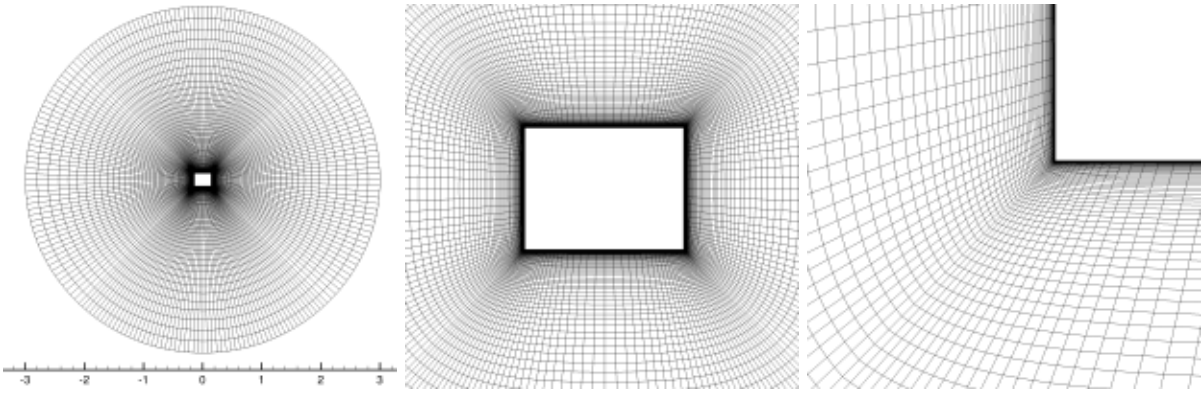

(a) Full domain (b) Zoom on the hull (c) Zoom on the bilge

Figure 3: Overview of the computational grid used for the section with sharp bilges

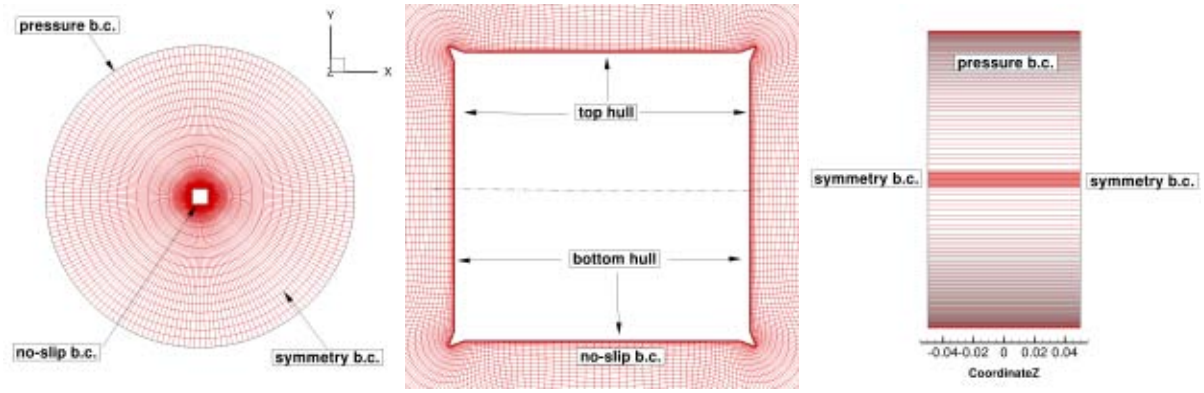

(a) Front View (b) Zoom on the hull (c) Side view

Figure 4: Boundary conditions used for all computations.

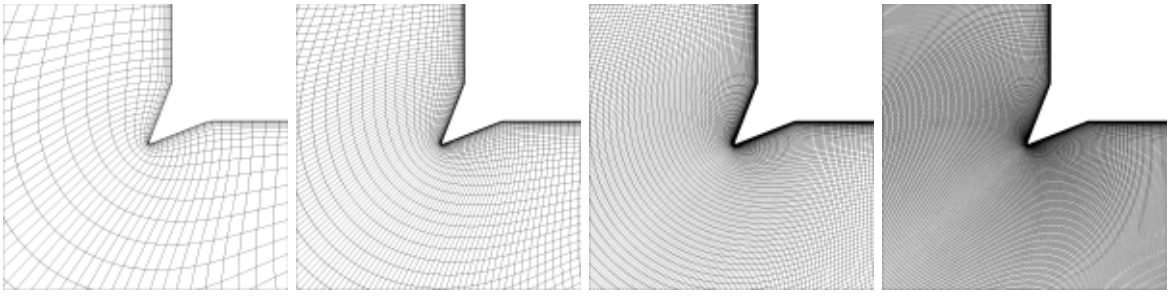

(a) Coarse (b) Medium (c) Fine (d) Very fine

Figure 5: Details of the GridPro grid in the vicinity of the bilge.

4.2 Boundary and initial conditions

The boundary conditions used are shown in Figure 4(b). A no-slip b.c. is applied on the hull, symmetry b.c. are applied on the planes in z-direction, while a pressure b.c. is used at the circular border of the domain. The moment is monitored separately on the bottom and on the top hull. The reference pressure prescribed at the circular border of the domain is $0Pa$. The grid refinement at the no-slip b.c. was such that the y^+ remained lower than 1 for the model scale computations. When this is satisfied, no-wall functions are applied. As initial conditions, the domain is full of water and the pressure and velocity components are set to zero in all cells. The roll angle of the hull section at the beginning of the computation is null.

4.3 CFD code

ReFRESCO is a MARIN in-house viscous-flow CFD code [15]. It solves the multi-phase unsteady incompressible RANS (Reynolds-averaged Navier-Stokes) equations, complemented with turbulence models and volume-fraction transport equations for different phases. The equations are discretized using a finite-volume approach with cell-centered collocated variables. The implementation is face-based, which permits grids with elements consisting of an arbitrary number of faces (hexahedrals, tetrahedrals, prisms, pyramids, etc.), and if needed h-refinement (hanging-nodes). The code is parallelized using MPI and sub-domain decomposition, and runs on Linux workstations, clusters and super-computers. The code is targeted, optimized and validated, exclusively for hydrodynamic applications. It has already been applied, verified and validated for several offshore typical flows, in particular for current and maneuvering coefficients of semi-submersibles, submarines and ships and wind loads. [16, 17, 18, 19, 20].

For the problem here treated the RANS equations are solved using a so-called *Absolute-Formulation or ABF*. This means that the velocity vector $\mathbf{V}$ is defined in the absolute or inertial earth-fixed reference frame, with the equations being solved in the body-fixed reference frame which is moving with velocity $\mathbf{V_d} = \omega \times \mathbf{r} + \mathbf{V_s}$. No free-surface effects are considered but flow is considered to be turbulent. The URANS equations read then:

$$\nabla \cdot (\mathbf{V} - \mathbf{V_d}) = 0, \tag{14}$$

$$\begin{aligned} \frac{\partial (\rho V_i)}{\partial t} + \nabla \cdot [\rho (\mathbf{V} - \mathbf{V_d}) V_i] &= \nabla \cdot \left[(\mu + \mu_t) \left(\nabla \mathbf{V} + \nabla \mathbf{V}^T \right) \mathbf{i_j} \right] - \nabla (p + \frac{2}{3} \rho k) \mathbf{i_i} \\ &- \rho (\omega \times \mathbf{V}), \end{aligned} \tag{15}$$

where μ_t, k are determined by a turbulence model and $i, j = 1, \cdots, 3$. In the specific case here dealt with, there is no translation velocity $\mathbf{V_s} = 0$ and therefore $\mathbf{V_d} = \omega \times \mathbf{r}$, with $\omega = (0, 0, \phi')$ and ϕ' derived from Equation 6. The advantages of using a ABF formulation are: 1) moving-grid algorithms are not needed, which decreases the CPU time needs; 2) the variables are defined in the earth-fixed reference frame and therefore there is no need for additional post-processing; 3) the usual Coriolis and centrifugal forces are no longer added explicitly to the right-hand-side of the equations, which eases the iterative convergence of the calculations. For this ABF method, boundary conditions must be defined in the earth-fixed reference frame. The same method is used at MARIN for calculations of open-water propeller characteristics with moderate CPU time costs and good iterative convergence properties [21].

4.4 Numerical settings

A forced roll motion is prescribed to the hull section, and the start-up function is applied for T_F=4 periods. Unsteady computations are carried out to solve momentum, continuity and turbulence equations. All simulations are twenty roll periods long and the harmonic-analysis method is performed on the 10 last periods of the simulation, after transient effects disappeared. A three-time-level discretization scheme (2^{nd} order) with a fixed time step is used for all equations. Within each time step a RMS residual drop of 10^{-5} nominal value is attempted by carrying out several outer-loops with a maximum of 500, also tested here. For convection terms, in the momentum equation a QUICK scheme (2^{nd} order) is used, while in the turbulence equation an UPWIND scheme (1^{st} order) is employed. All gradients are calculated using Gauss' theorem (2^{nd} order). Unless stated otherwise, the calculations are performed with the $k - \omega$ SST turbulence model with an eddy-viscosity ratio μ_τ / μ equal to 1 and all other turbulent quantities automatically defined in ReFRESCO.

5 RESULTS FOR A RECTANGULAR HULL WITH SHARP BILGES

5.1 Grid and time-step sensitivity

The detailed grid and time step sensitivity studies for the rectangular hull section with sharp bilges have been reported in [5]. There, it was shown that the medium grid (containing 173K cells) is a good compromise between accuracy of the results and computational time. It is also concluded that the time step to be used should be at least $\Delta t = T/800$. In this paper, the results presented are obtained using this grid and time step.

5.2 Iterative convergence sensitivity

In [5] it was shown that the iterative convergence had a significant influence on the results. Here, the iterative convergence of the computations is further improved. Within each time step, a RMS residual drop of 10^{-3} nominal value is attempted by carrying out several outer-loops with a maximum of 500. Figure 6(a) shows the residual behavior during two time steps, the so-called *"unsteady residuals"*. The x-axis represents the total number of outer-loops during the simulation while the y-axis represents the infinity norm, L_∞, of the residuals. It can be seen that the residuals are clearly decreasing with the outer-loops, and the convergence tolerance is fulfilled after less than 30 outer-loop iterations. Figure 6(b) shows the the so-called *"steady residuals"*. The x-axis shows the number of time steps while the y-axis shows the residuals obtained at the last outer-loop iteration of each time step. This figure confirms that the convergence criteria is fulfilled most of the time. The turbulent kinetic energy residuals are sometimes higher than 10^{-3}. This happens very locally, when the velocity of the hull section is close to null. Due to the quality of the ICEM-CFD grids, better iterative convergence was difficult to obtain. Nevertheless, note that the L_2 RMS norm of the residuals is in general two orders lower that the L_∞ norm.

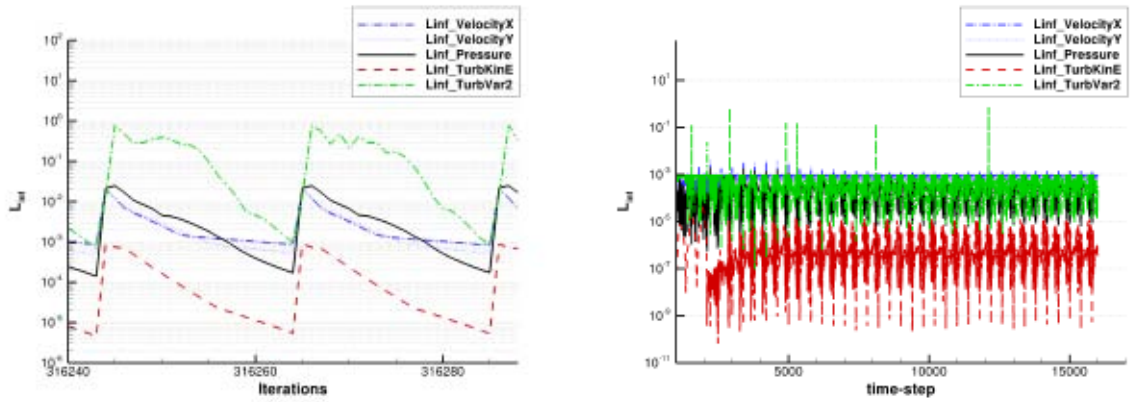

(a) *"Unsteady"* residuals

(b) *"Steady"* residuals

Figure 6: Iterative convergence for $\phi_0 = 0.132rad$ and $T = 1.5s$.

5.3 Influence of the roll amplitude

All combinations of amplitudes and periods tested by Ikeda in [1] for the rectangular hull shape with sharp bilges are here simulated. The wave damping is calculated with a potential flow code DIFFRAC and results are reported in [5]. The total damping is assumed to be the sum of the wave damping determined by DIFFRAC and the viscous damping determined by ReFRESCO. The equivalent linear-damping coefficients obtained numerically is compared to the experimental values. Figure 7(a) compares the hydrodynamic moments computed on the bottom hull for a roll period $T = 1.0s$ and four different amplitudes. It shows that the moment amplitude is drastically increasing with the amplitude. It is also interesting to notice that the shape of the moment time trace varies for different amplitudes. The phase of the moment curve seems not to be significantly affected by the amplitude. Figure 7(b) represents the damping coefficients as a function of the roll amplitude. It shows a very good agreement between the

experimental results of Ikeda and the numerical results using CFD. This also confirms that the damping coefficient is linear with the roll amplitude. The experimental results show however some scatter from the linear trend. This is probably due to the uncertainty in the experimental results.

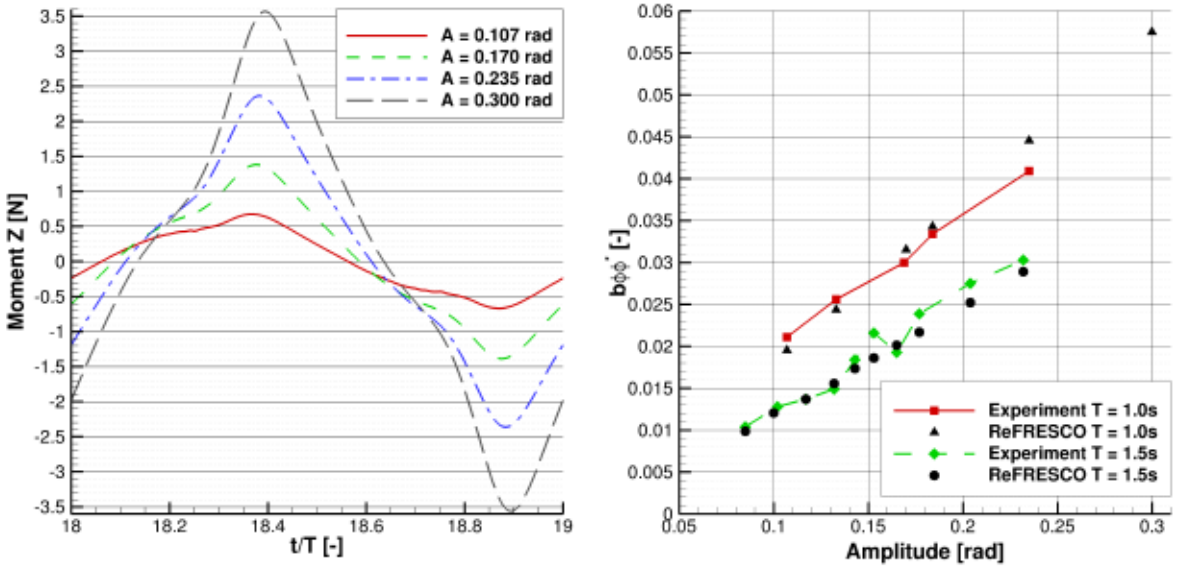

(a) Influence on the moment

(b) Influence on the damping coefficient

Figure 7: Influence of the roll amplitude on the moment and damping coefficients.

5.4 Flow analysis

Figure 8 shows the vorticity flow field at different instants of the last cycle of the simulation. A flow cycle can be characterized as follows:

- At $t = T$, two strong vortices of different sign are visible close to the bilge and one under the hull. The vorticity at the boundary-layer attached to the hull changes sign at a certain position of the hull.
- At $t = 1.2T$, the positive-vorticity vortex (red) has been shed to the upper left part of the picture. A new positive-vorticity vortex starts to be formed close to the edge of the hull.
- At $t = 1.4T$, the new positive-vorticity vortex (red) is now bigger and is located under the hull. The blue negative-vorticity vortex "escapes" the boundary-layer and slides over the red one. The maximum moment within this cycle is here achieved, which corresponds in Figure 7(a) to $t/T = 18.4$.
- At $t = 1.5T$, the hull is again at the zero-angle position. The vortices have grown but are still attached to each other.
- At $t = 1.7T$, the blue vortex has been shed and is now under the hull. This vortex is the same as the one seen for $t = T$ located under the hull.
- At $t = 1.8T$, a new negative-vorticity blue vortex starts to be formed at the left wall.
- At $t = 1.9T$, the negative-vorticity blue vortex grows and the positive-vorticity red vortex slides over it. The minimum moment within this cycle is achieved, which corresponds in Figure 7(a) to $t/T = 18.9$.
- At $t = 2.0T$, the flow field is the same as at $t = T$ and the complete procedure starts over again.

Section 5.3 showed that the damping coefficients are linearly increasing with the roll-motion amplitude. This viscous damping is mainly due to vortex formation at the sharp bilges, and it is therefore of interest to observe the flow near the bilges. The C_p field for the roll period $T = 1.0s$ and $T = 1.5s$ is shown for

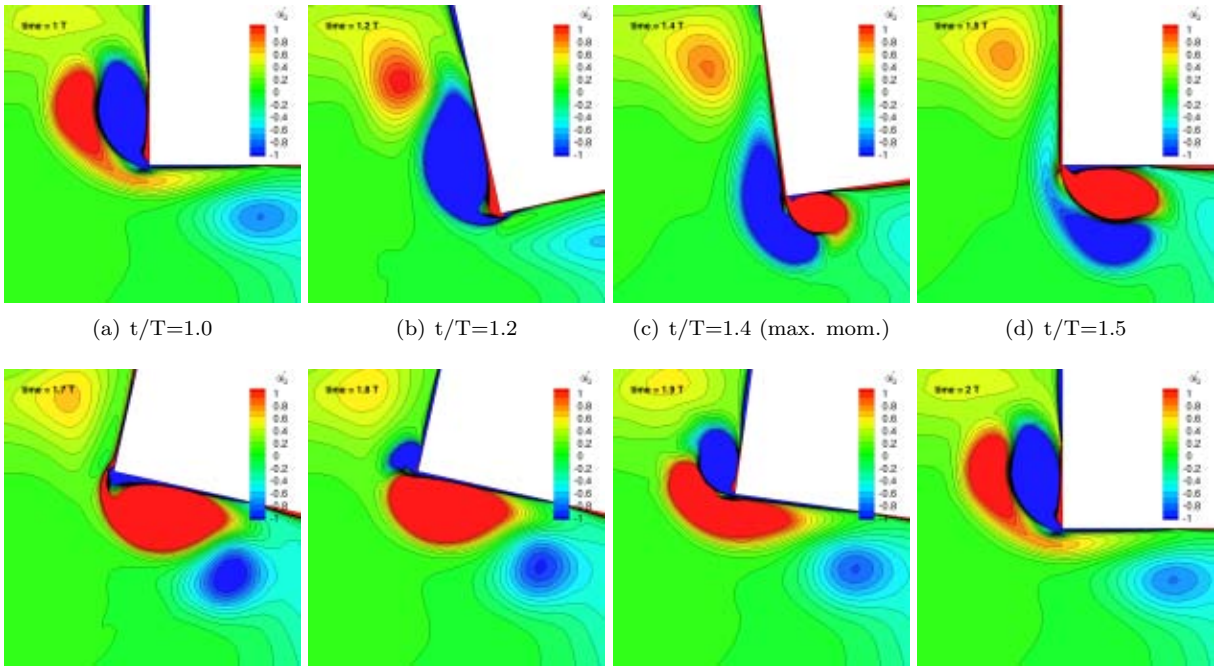

(a) t/T=1.0 (b) t/T=1.2 (c) t/T=1.4 (max. mom.) (d) t/T=1.5

(e) t/T=1.7 (f) t/T=1.8 (g) t/T=1.9 (min. mom.) (h) t/T=2.0

Figure 8: Vorticity field ω_z^* in the vicinity of the sharp bilge for various time steps within one cycle. $\phi_0 = 0.232rad$ and $T = 1.5s$.

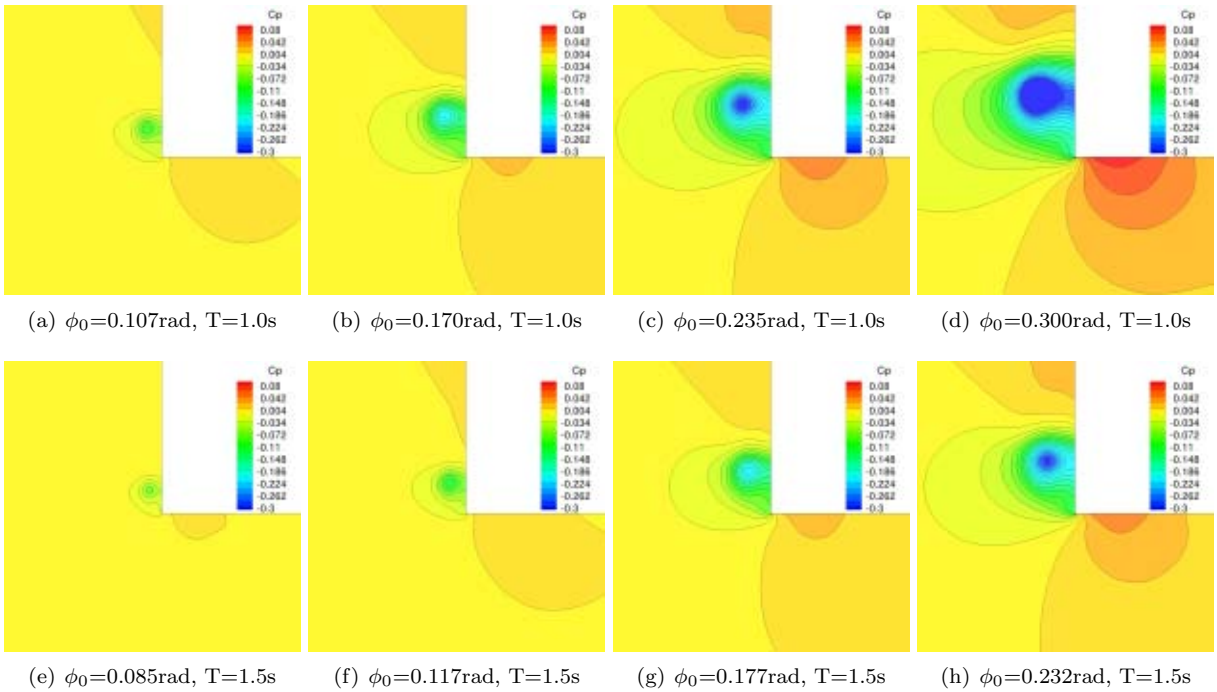

(a) ϕ_0=0.107rad, T=1.0s (b) ϕ_0=0.170rad, T=1.0s (c) ϕ_0=0.235rad, T=1.0s (d) ϕ_0=0.300rad, T=1.0s

(e) ϕ_0=0.085rad, T=1.5s (f) ϕ_0=0.117rad, T=1.5s (g) ϕ_0=0.177rad, T=1.5s (h) ϕ_0=0.232rad, T=1.5s

Figure 9: Pressure field C_p in the vicinity of the sharp bilge for various amplitudes and periods.

various amplitudes in Figure 9, for the instant of $0deg$ of roll angle, or $t = T$, for the last simulation cycle. The ω_z^* field for the roll period $T = 1.0s$ and $T = 1.5s$ is shown for various amplitudes in Figure 10. In

these two Figures, the roll amplitude is increasing from the left side to the right side, and the roll period from top to bottom. It appears that the amplitude has a large influence on the pressure and vorticity field. It is clear, that the size of the vortices significantly increases with the amplitude. The influence of the period is barely visible both in the vorticity and the pressure field.

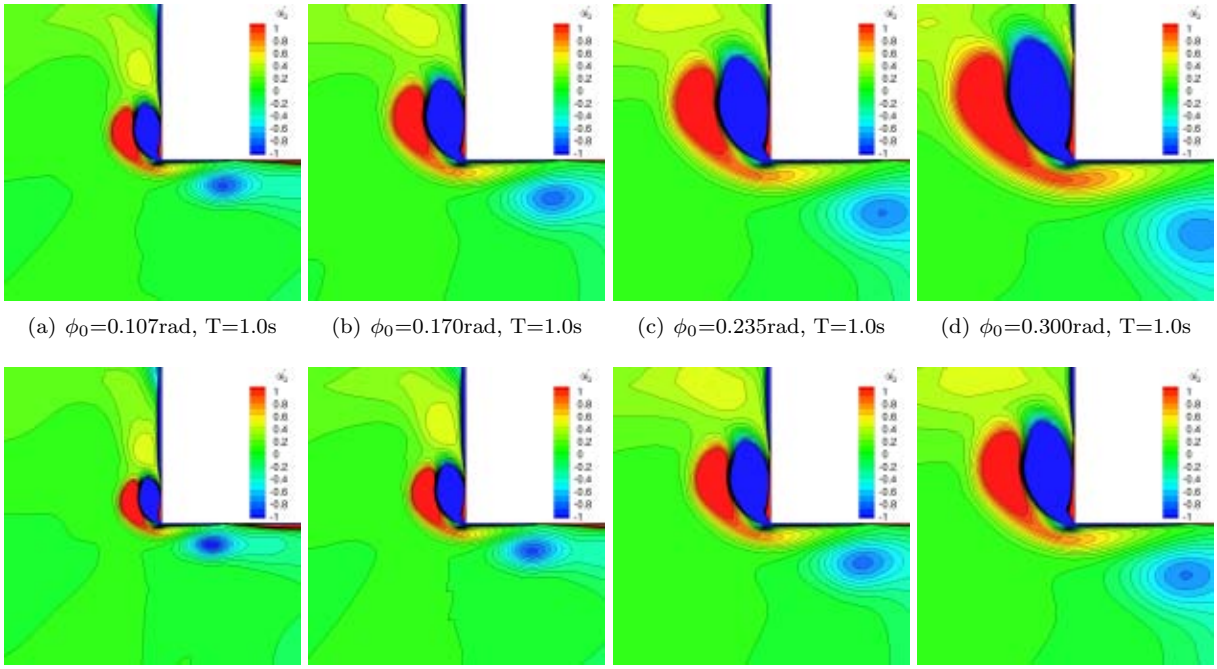

(a) ϕ_0=0.107rad, T=1.0s (b) ϕ_0=0.170rad, T=1.0s (c) ϕ_0=0.235rad, T=1.0s (d) ϕ_0=0.300rad, T=1.0s

(e) ϕ_0=0.085rad, T=1.5s (f) ϕ_0=0.117rad, T=1.5s (g) ϕ_0=0.177rad, T=1.5s (h) ϕ_0=0.232rad, T=1.5s

Figure 10: Vorticity field ω_z^* in the vicinity of the sharp bilge for various amplitudes and periods.

6 RESULTS FOR A RECTANGULAR HULL WITH BILGE KEELS

6.1 Iterative convergence sensitivity

Residual drops of 10^{-2}, 10^{-3}, 10^{-4} and 10^{-5} (L_∞ norm) are attempted with a maximum of 500 iterations per outer-loop, and the influence of this convergence tolerance on the results is investigated. Figure 11 shows the residual behavior for one computation with a convergence tolerance 10^{-4}. The fine grid and a time step $\Delta t = T/800$ are used. It can be seen that the residuals are decreasing with the number of outer-loops, till the threshold of 10^{-4} is reached. Figure 11(b) shows that a good convergence is achieved for all times-steps. The superior quality of the GridPro grid plays also a role in the better iterative convergence in this case than in the previous one. Figure 12 shows the dependency of the damping coefficients to the convergence tolerance. It shows that a convergence tolerance of at least 10^{-4} (L_∞ norm) should be achieved at each time step to obtain a converged solution. The pressure field (not shown here) show differences for the convergence tolerances between 10^{-2} and 10^{-4}. Very few differences can be observed between the tolerances 10^{-4} and 10^{-5}.

6.2 Grid and time-step sensitivity

Grid and time-step sensitivity studies are here carried out for the amplitude $\phi_0 = 0.1rad$ and period $T = 1.55s$. Figure 13(a) shows the moment time trace calculated on the bottom hull section during the ninetieth period. It shows that the calculated moment does not vary much with the grid refinement. The calculated moments for the medium and fine grid are very similar. However, Figure 13(b) shows that the damping coefficient is significantly affected by the grid refinement. On this figure, the viscous damping coefficient for all grids and time steps is presented. The damping coefficient does not show significant change for smaller time steps, but a clear decrease is observed for finer grids. Based on this, it was

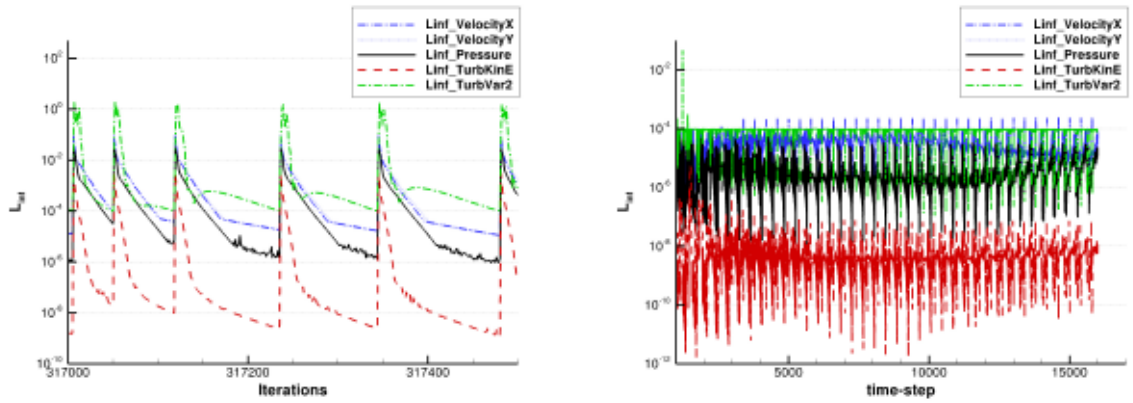

(a) *"Unsteady residuals"* (b) *"Steady residuals"*

Figure 11: Iterative convergence for $\phi_0 = 0.1rad$ and T=1.55s at model scale Re_{ms}.

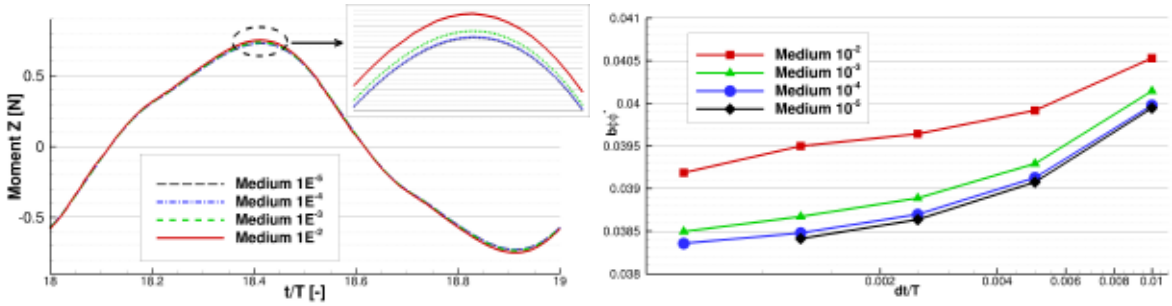

(a) Influence on moment (b) Influence on damping coefficient

Figure 12: Influence of the iterative convergence on moment (left) and viscous damping coefficient (right).

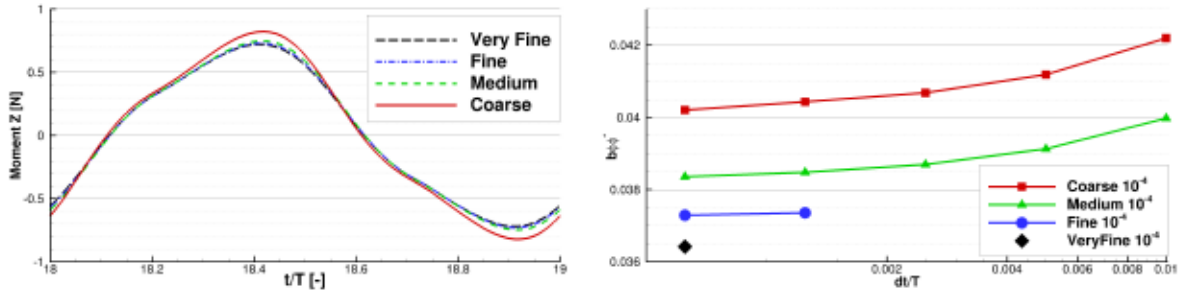

(a) Influence on moment ($\Delta t = T/800$) (b) Influence on the damping coefficient

Figure 13: Influence of the grid and time-step refinement on moment (left) and viscous-damping coefficient (right). The iterative convergence is 10^{-4}.

decided to perform the following calculations using the fine grid and the time step $T/800$. A finer grid would provide more accurate results though. In the future, a verification and validation (V&V) procedure presented in [7] will be applied. With this procedure, a numerical uncertainty can be determined and the sensitivity of the solution to grid and time step can be better quantified.

6.3 Influence of turbulence model

According to the experience of the authors, and within the URANS framework, the eddy-viscosity based $k-\omega$ SST turbulence model is an optimal choice between complexity and turbulence modelling [22, 23]. Nevertheless, in order to investigate the influence of turbulence modelling on the results for the damping coefficients, one computation with the also-known one-equation Spalart-Allmaras (SA) turbulence model [24] is carried out. This is done for the roll amplitude $\phi_0 = 0.1rad$, period $T = 1.55s$, using the fine grid and a time-step size $\Delta t = T/800$. The viscous damping coefficients obtained with $k-\omega$ and SA turbulence models are respectively $b^*_{\phi\phi} = 0.03741$ and $b^*_{\phi\phi} = 0.03917$, i.e. a difference of about 4.5%. The differences are larger than any so far presented, and are also present on the calculated moment time traces (not shown here). This can be explained by considering the calculated flow solution. Figure 14 shows the influence of the turbulence model on the calculated pressure and vorticity fields. The vortices are seen to be more circular and stronger in the results obtained with the SA turbulence model. This explains the difference on the damping coefficients. For the following calculations the $k-\omega$ SST model is used.

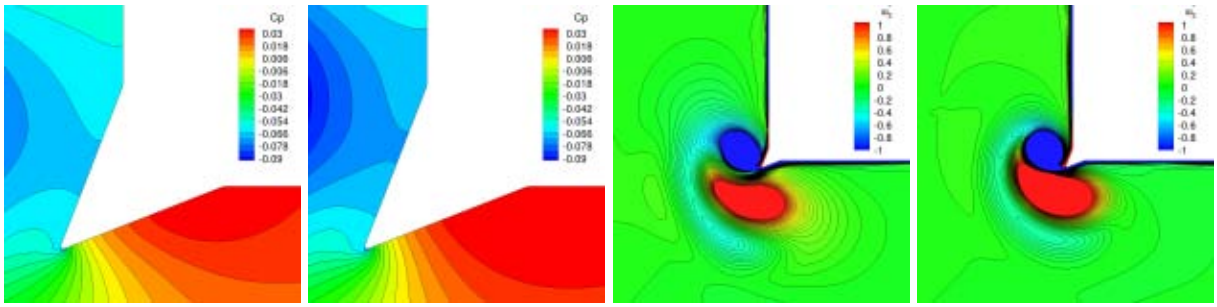

(a) $k-\omega$ model (b) SA model (c) $k-\omega$ model (d) SA model

Figure 14: Influence of the turbulence model on the C_p and ω^*_z flow field for $\phi_0 = 0.1rad$ and $T = 1.55s$.

6.4 Influence of the roll period

In order to investigate the influence of the roll period on the hydrodynamic moment and damping coefficients, calculations are performed for the periods tested in [3, 4] at a fixed amplitude of $\phi_0 = 0.1rad$. Figure 15(b) compares the damping coefficients as a function of the dimensionless frequency. On this figure, the viscous damping calculated by ReFRESCO is compared to the total damping measured in [3, 4]. Clearly, the numerical results show that the viscous damping increase linearly with the roll frequency. This confirms the results of Ikeda [11] which states that the eddy damping is a linear function of the roll frequency for frequencies lower than $\omega^* = 0.6$. A reasonable agreement is found for frequencies lower than $\omega^* = 0.7$. At the period $T = 1.55s$ or frequency $\omega^* = 0.505$, at which all sensitivity studies have been carried out, the difference between the numerical and experimental results is of 6.9%. However, the numerical results deviate considerably from the experimental values for frequencies higher than 0.7. Figure 15(a) shows the influence of the roll period on the hydrodynamic moment computed on the bottom hull section. The x-axis shows the period at which the moment time trace is shown. Here the ninetieth period is plotted. It can be seen that the moment amplitude is increasing when the period is decreasing, without large deviations in the moment curve, which explains the linearity of the damping coefficients observed. The free-surface contribution is not taken into account here. However, this contribution calculated by a potential-flow code is small and positive, which will further increase the difference with the experiments here shown. Two explanations are possible: 1) the linearization here done (independent free-surface and other flow contributions), and considered by the classical methods and authors such as Ikeda, is not valid for this case and for large frequencies; 2) there is some inaccuracy in the experiments. Hypothesis 1 will be verified by performing the same calculations with free-surface modelling. RANS results considering free-surface effects presented by other authors [25], obtained with two different codes, show the non-linear decrease of the damping-coefficient for large frequencies not captured with the present approach. Nevertheless, the results presented in [25] clearly over-predict the damping coefficients of the experiments for all frequencies. This deserves further investigation.

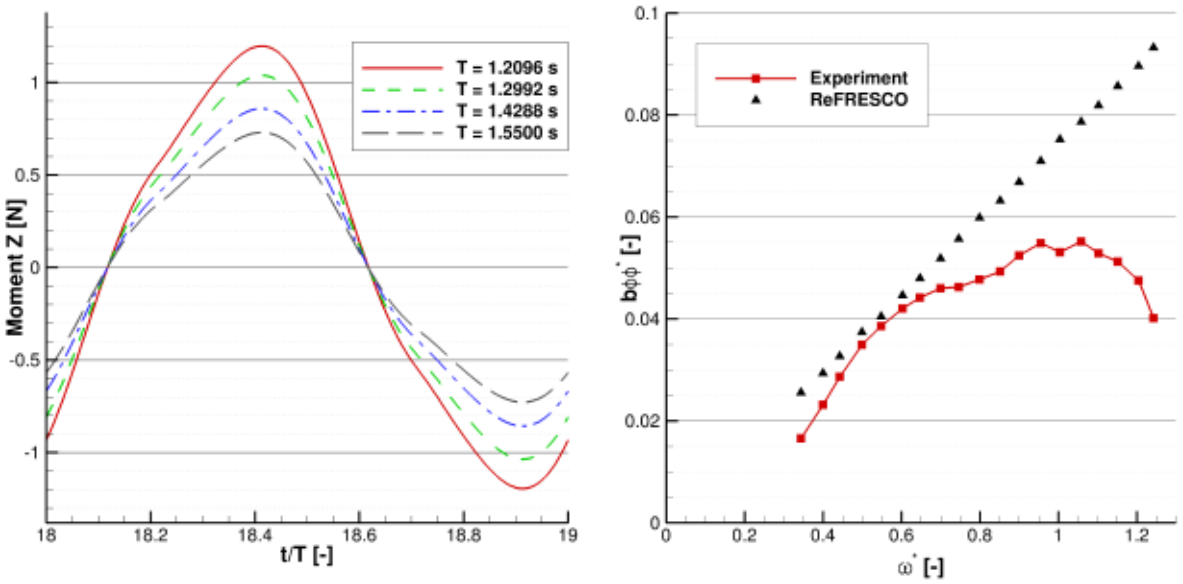

(a) Influence on the moment

(b) Influence on the damping coefficient

Figure 15: Influence of the roll period on the moment and damping coefficients.

6.5 Flow analysis

Figure 16 shows that one flow cycle presents several differences with respect to the hull without bilge keels. The two vortices, one with positive and other with negative-vorticity strength, still exist but are

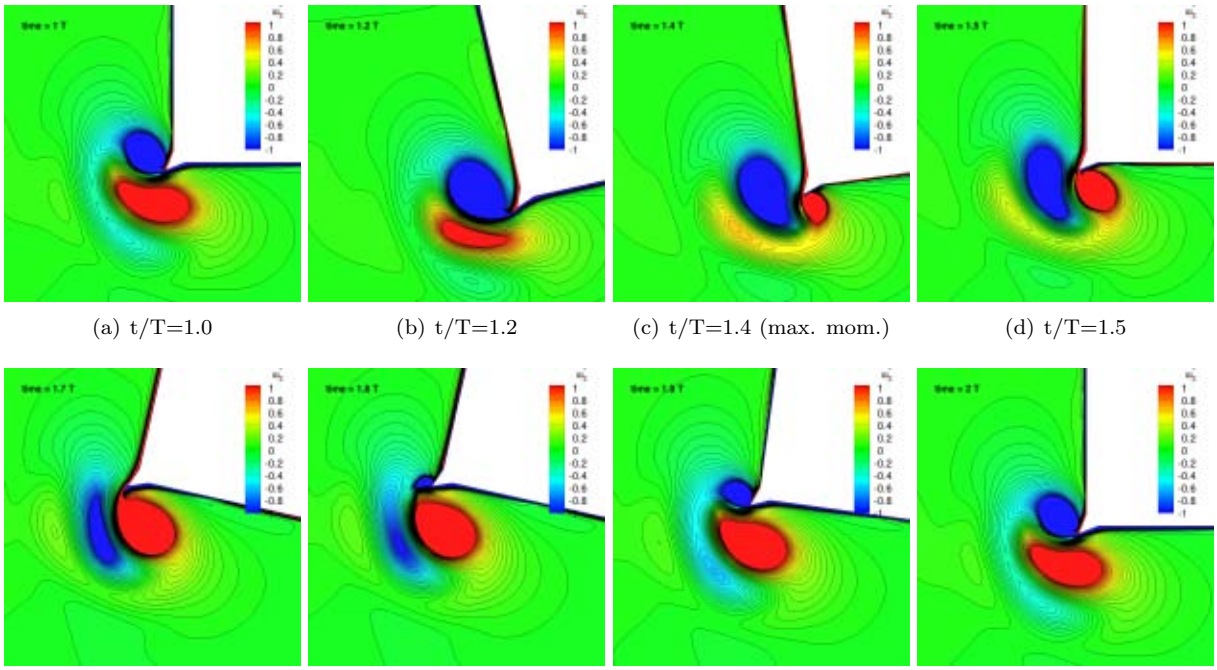

(a) t/T=1.0 (b) t/T=1.2 (c) t/T=1.4 (max. mom.) (d) t/T=1.5

(e) t/T=1.7 (f) t/T=1.8 (g) t/T=1.9 (min. mom.) (h) t/T=2.0

Figure 16: Vorticity field ω_z^* in the vicinity of the sharp bilge for various time steps within one cycle. $\phi_0 = 0.1rad$ and $T = 1.55s$.

mostly attached to the bilge keels. The vortices are not shed easily to other parts of the flow field. The complete flow pattern is determined by the shape and size of the bilge keel.

6.6 Preliminary study of scale effects

So far, the computations presented have been performed for a model scale Reynolds number $Re_{ms} = 2.7 \times 10^5$. In order to investigate possible scale effects on the viscous roll damping, the computation for an amplitude $\phi_0 = 0.1rad$ with a period of $T = 1.55s$ is performed for a full-scale Reynolds number $Re_{fs} = 9.4 \times 10^7$ (scale 50). The fine grid is used with a time step $\Delta t = T/800$. Residual drops of 10^{-4} (L_∞ norm) are aimed for with a maximum of 500 outer-loop iterations per time step. In this preliminary stage of the study, the same grid used for the model-scale calculations is here used and, therefore, y^+ is less than 80. This means that wall functions are used in the full-scale computations, which adds an extra modelling inaccuracy. This deserves further investigation.

Figure 17 shows the residuals convergence for the full-scale calculation. By comparing Figure 17(a) to Figure 11(a), it appears that more outer-loops per time step are needed to fulfil the same convergence criteria of 10^{-4}. Figure 17(b) shows that this criteria is exceeded periodically. This only happens locally for a few time steps, when the angular velocity of the body is zero. In [26] it has been shown that these local high residuals do not have a significant influence on the calculated viscous damping.

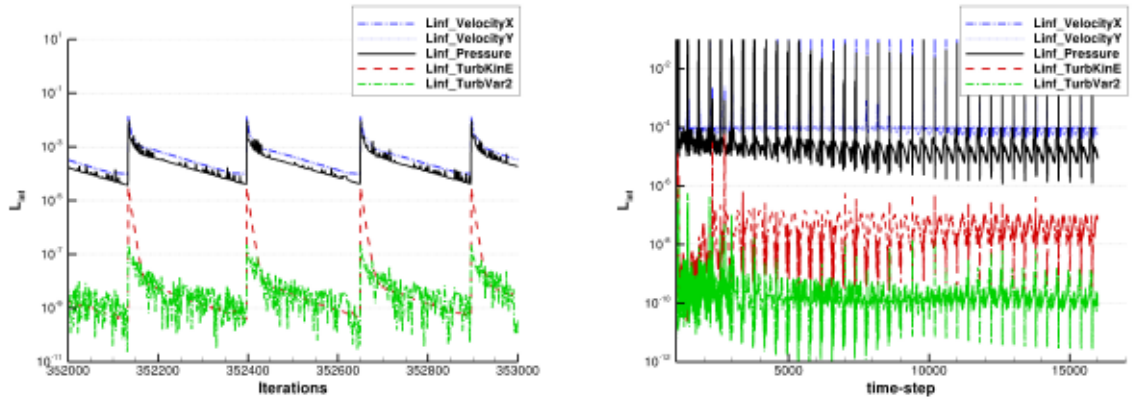

(a) *"Unsteady residuals"* (b) *"Steady residuals"*

Figure 17: Iterative convergence for $\phi_0 = 0.1rad$ and $T = 1.55s$ at full scale Re_{fs}.

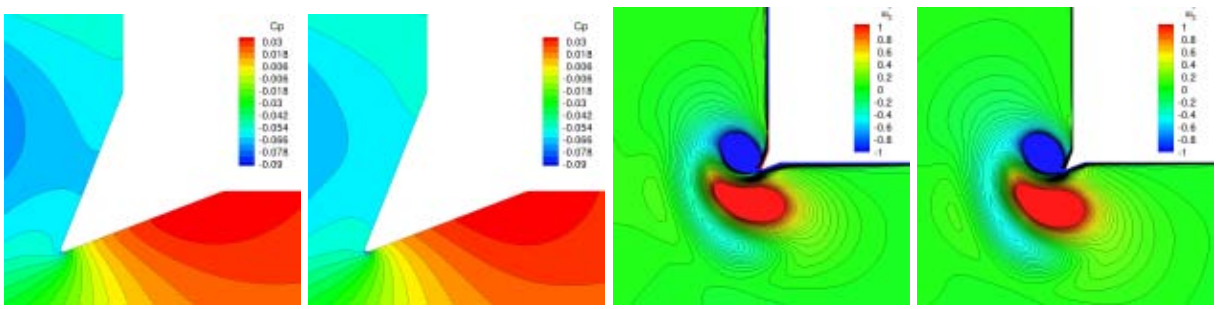

(a) model-scale C_p (b) full-scale C_p (c) model-scale ω_z^* (d) full-scale ω_z^*

Figure 18: Scale effects on pressure and vorticity fields in the vicinity of the bilge keel.

Figure 18 compares the C_p and ω_z^* fields between model-scale and full-scale calculations. No clear differences can be noticed, except near the boundary layer, which is obviously thinner. This similarity

of the flow is confirmed by the analysis of the damping coefficients. The viscous-damping coefficient for the model-scale computation is $b^*_{\phi\phi} = 0.03741$, while at full scale is $b^*_{\phi\phi} = 0.03797$. This is about 1.5% difference. Even if numerical uncertainties have not be considered, that wall-functions have been used, and that more frequencies and amplitudes should be considered, the scale effects on the viscous-damping coefficient seem to be negligible for this particular case. One reason for this could be that the separation point of the vortices is fixed at the end of the bilge keel and therefore fairly independent of the Reynolds number.

7 CONCLUSIONS AND FUTURE WORK

In this paper MARIN's URANS code ReFRESCO has been used for roll-damping applications. The unsteady flow around a forced rolling hull section with and without bilge keels is computed. Extensive numerical sensitivity studies are carried out and the viscous-damping coefficient is computed for various roll amplitudes and periods. The numerical results of ReFRESCO are compared to available experimental values. A double-body approach has been used, which corresponds to a linearization of the problem with respect to the free-surface, following the classical approach by Ikeda [1].

Generally, the influence of the grid resolution on the viscous damping coefficient is significant, and relatively fine grids (order of 100KCells for a 2D calculation without free-surface) should be used to obtain a grid-converged solutions, even using second-order discretization schemes for convection and diffusion terms. The viscous-damping coefficient decreases when the grid is refined. The influence of the time step is smaller but a time step of at least $\Delta t = T/800$ is recommended. The influence of the iterative convergence is obviously visible on the flow pattern and on the calculated viscous-damping coefficients. It is shown that an iterative convergence level of 10^{-4} in the L_∞ norm, for all quantities, is a good compromise between accuracy of the results and computational time. However, this is very much dependent on code, iterative solver and residual normalization, and therefore this conclusion cannot be considered general for all CFD tools.

The numerical results obtained with the potential-flow diffraction code DIFFRAC, for the free-surface damping, and ReFRESCO, for all other components, for the rectangular hull with sharp bilges have been compared to the classical experimental values by Ikeda [1]. Two periods were calculated for various roll amplitudes. A very good agreement has been found, with deviations lower than 10% for all amplitudes and the two periods. For this case, it is confirmed that the viscous-damping coefficient is linear with the roll amplitude. The computed flow fields also show that the vortices generated at the bilges are larger when the amplitude is increasing.

The numerical results obtained with ReFRESCO for the rectangular hull with triangular-shaped bilge keels have been compared to the experimental results of Yeung [3]. The influence of the grid and time step refinement, iterative convergence and turbulence models have been investigated. Poor grid and time step refinements, or poor iterative convergence leads to overestimated damping coefficients. A 160K cells grid, with a time step $\Delta t = T/800$ has been used to calculate the flow for one amplitude and various periods. The free-surface or wave-damping component calculated by potential-flow tools is negligible for this case. A reasonable agreement between ReFRESCO and the experimental data is found for dimensionless frequencies lower than 0.7. For these values a deviation from the experimental values lower than 10% is observed. For the case $\phi_0 = 0.1rad$ with $\omega^* = 0.505$, for which all sensitivities studies were carried out, the difference between the numerical and experimental results is about 6.9%. For dimensionless frequencies higher than 0.7, the viscous-damping coefficient calculated highly overestimates the model-tests results. Furthermore, the calculated viscous damping is linear with the frequency. The damping from the experiments is not linear with the frequency for frequencies higher than $0.6 - 0.7$. In the near future, CFD computations including the free surface will be performed, and these results will be further investigated.

For the hull section with bilge keels, a preliminary study on possible scale effects has been performed. Using the best numerical settings obtained for model scale, one calculation (one amplitude and frequency) has been performed for a full-scale Reynolds number corresponding to a geometrical scale factor of 50. The preliminary results showed that the pressure and vorticity fields are very similar for both model and full-scale for this particular case. The difference in viscous-damping coefficients is of 1.9%. This deserves further investigation, and both more detailed numerical studies and physical conditions should be considered before a final conclusion can be drawn on scale/Reynolds effects for roll viscous-damping

coefficients.

Future work to be done involves mainly the following topics: 1) the influence of free-surface in the 2D flow around rolling hull sections and associated viscous and total-damping coefficients; 2) further study of possible scale effects; 3) full 3D calculations without and with free-surface. We also emphasize that in the short term, modern verification and validation techniques [6, 7] will be utilized in order to further assess, and better quantify, the quality of the numerical results for the viscous and total- damping coefficients.

REFERENCES

[1] Y Ikeda, Y. Himeno, and N. Tanaka. Components of Roll Damping of Ship at Forward Speed. *JSNA Japan*, 143, 1978.

[2] Y. Himeno. Prediction of Ship Roll Damping, State of the Art. Technical Report 239, University of Michigan, 1981.

[3] R.W. Yeung, S.W. Liao, and D. Roddier. Hydrodynamic Coefficients of Rolling Rectangular Cylinders. *International Journal of Offshore and Polar Engineering*, Vol.8.No.4, 1998.

[4] R.W. Yeung, D. Roddier, B. Allessandrini, L. Gentaz, and S.W. Liao. On Roll Hydrodynamics of Cylinders Fitted with Bilge Keels. In *Twenty-third symposium on naval hydrodynamics*, number 863-880, 2001.

[5] F. Jaouen, A. Koop, and G. Vaz. Predicting Roll Added Mass and Damping of a Ship Hull Section using CFD. In *Proceedings of ASME 30th International Conference on Ocean, Offshore and Arctic Engineering OMAE2011*, number OMAE2011-49085, 2011.

[6] L. Eça, G. Vaz, and M. Hoekstra. Code Verification, Solution Verification and Validation in RANS Solvers. *In Proceedings of OMAE2010, Shanghai, China*, June 2010.

[7] F. Fathi, L. Eça, and M Borsboom. An Example of Code Verification in the Simulation of Wave Propagation. *In Proceedings of OMAE2011, Rotterdam, the Netherlands*, June 2011.

[8] J.M. Journee and W.W. Massie. *Offshore Hydrodynamics*. Delft University of Technology, first edition, 2001. Chapter 12.

[9] J.A. Pinkster and R.H.M. Huijsmans. Wave Drift Forces in Shallow Water. *BOSS1992*, 1992.

[10] S. Martin. Validation and Verification of ReFRESCO for Viscous Flows around Rolling Structures with Bilge Keels. Master's thesis, Ecole Centrale de Nantes; MARIN, 2011.

[11] Y. Ikeda, Y. Himeno, and N. Tanaka. On Eddy Making Component of Roll Damping Force on Naked Hull. *Report of Department of Naval Architecture University of Osaka Prefecture*, No. 00403, 1978.

[12] F. Chanony. Validation and Verification of FreSCo for Viscous Flows around Oscillating Bodies: Roll Motion. Internship report, MARIN, 2009.

[13] http://www.ansys.com/products/icemcfd.asp.

[14] http://www.gridpro.com/.

[15] G. Vaz, F. Jaouen, and M. Hoekstra. Free-Surface Viscous Flow Computations. Validation of URANS Code FreSCo. *In Proceedings of OMAE2009, Honolulu, Hawaii, USA*, June 2009.

[16] G. Vaz, O. Waals, F. Fathi, H. Ottens, T. Le Souef, and K. Kwong. Current Affairs - Model Tests, Semi-Empirical Predictions and CFD Computations for Current Coefficients of Semi-Submersibles. *In Proceedings of OMAE2009, Honolulu, Hawaii, USA*, June 2009.

[17] S.L. Toxopeus and G. Vaz. Calculation of Current or Manoeuvring Forces using a Viscous-Flow Solver. *In Proceedings of OMAE2009, Honolulu, Hawaii, USA*, June 2009.

[18] F. Fathi, C.M. Klaij, and A. Koop. Predicting Loads On a LNG Carrier with CFD. *In Proceedings of OMAE2010, Shanghai, China*, June 2010.

[19] A. Koop, C.M. Klaij, and G. Vaz. Predicting Wind Shielding for FPSO Tandem Offloading using CFD. *In Proceedings of OMAE2010, Shanghai, China*, June 2010.

[20] G. Vaz, S.L. Toxopeus, and S. Holmes. Calculation of Manoeuvring Forces on Submarines Using Two Viscous-Flow Solvers. *In Proceedings of OMAE2010, Shanghai, China*, June 2010.

[21] D. Rijpkema and G. Vaz. Viscous Flow Computations on Propulsors: Verification, Validation and Scale Effects. *In Proceedings of RINA-CFD2011, London, UK*, March 2011.

[22] Von Karman Institute for Fluid Dynamics. *Introduction to Turbulence Modelling*, 2004.

[23] Von Karman Institute for Fluid Dynamics. *LES and Related Techniques*, 2008.

[24] P. Spalart and S. Allmaras. A One-Equation Turbulence Model for Aerodynamic Flows. *In the Proceedings of AIAA 30th Aerospace Sciences Meeting, Reno, Nevada, USA*, (AIAA92-0439), 1992.

[25] Y.H. Yu. *Prediction of Flows around Ship-shaped Hull Sections in Roll Using an Unsteady Navier-Stokes Solver*. PhD thesis, The University of Texas at Austin, August 2008.

[26] P. Crepier. Validation of an URANS CFD code ReFRESCO - Roll Damping Simulations. Internship Report, MARIN, 2011.